INSTITUTE OF PLASMA PHYSICS

NAGOYA UNIVERSITY

NONLINEAR SKIN EFFECT OF HIGH-POWER MICROWAVE INCIDENT ON A COLLISIONLESS MAGNETIZED PLASMA

K. Minami*, K. P. Singh*,
M. Masuda* and K. Ishii

IPPJ-194 August 1974

RESEARCH REPORT

NAGOYA, JAPAN

NONLINEAR SKIN EFFECT OF HIGH-POWER MICROWAVE INCIDENT ON A COLLISIONLESS MAGNETIZED PLASMA

K. Minami*, K. P. Singh*,
M. Masuda* and K. Ishii

IPPJ-194 August 1974

Further communication about this report is to be sent to the Research Information Center, Institute of Plasma Physics, Nagoya University, Nagoya, 464, Japan.

Permanent address:
* Department of Electrical Engineering, Nagoya University, Nagoya, 464, Japan.

ABSTRACT

Experimental results are presented which verify a nonlinear skin effect of high-power microwaves incident on a collisionless, uniform plasma having a sharp boundary. The skin depth, observed by microwave reflection techniques, increases with the incident microwave power. The results are compared with the theoretical analysis in which the radiation pressure due to electromagnetic field is taken into account.

I. INTRODUCTION

Interaction between a powerful electromagnetic wave and a collisionless plasma is one of the important problems of plasma physics, in connection with laser and/or rf heating of plasmas. In recent years, several experiments have been reported on the nonlinear phenomena[1,2] associated with microwaves in collisionless plasmas. These phenomena were related to the parametric decay processes.

In 1969, Gekker and Sizukhin[3] measured the reflection coefficient of high-power microwaves incident on a nonuniform plasma in a circular waveguide. The plasma frequency at the maximum density was much greater than the microwave angular frequency. The reflection coefficients from the plasma decreased with increasing incident power. The anomalous absorption they observed was attributed by Kaw et al.[4] to a parametric excitation of ion waves through which the microwave was scattered into longitudinal plasma modes. It should be emphasized, however, that the experiment by Gekker and Sizukhin was carried out under somewhat incomplete conditions from our viewpoint. First, the theoretical analysis for the penetration of electromagnetic fields becomes more or less qualitative for such a nonuniform plasma. Second, they detected only the amplitude of the reflected power. Therefore, one could not know whether or not there was nonlinear penetration for a strong incident microwave.

In this article, we describe the experimental results for the nonlinear skin effect of high-power microwave

incident on a collisionless plasma. Although predicted by theory, this article presents what seems to be the first quantitative experiment where the skin depths of the microwaves are observed to be dependent on the incident power. In the present experiment, a semi-infinite uniform plasma is used in order to make the theoretical analysis tractable. The microwave reflection techniques[5] are applied to observe the skin depth.

II. THEORETICAL CONSIDERATIONS

Silin[6] developed a nonlinear theory for the reflection of plane monochromatic electromagnetic waves incident normally on the surface of a uniform fully-ionized plasma. Considerations are limited to a collisionless plasma above the cut-off density. Taking into account the radiation pressure on the plasma due to the electromagnetic field, the phase angle θ of the reflection coefficient is given by

$$\cos^2\frac{\theta}{2} = -\frac{1}{b}\ln\left[1 - b/(\omega_p/\omega)^2\right] \qquad (1)$$

where

$$b = 4\,(E_i/E_c)^2\,, \quad E_c^2 = 2m\omega^2\kappa T_e/e^2\,,$$

ω_p and ω are the plasma and microwave angular frequencies, E_i and E_c are the amplitudes of the incident wave and the critical electromagnetic field, respectively. As is shown in Eq.(1), the cut-off density, i.e., when $\theta = 0$ is given

by $(\omega_p/\omega)^2 = b/(1 - e^{-b})$, which becomes, respectively, $1/(1 - b/2 + \cdots)$ and b for $b \ll 1$ and $b \gg 1$. Equation (1) reduces to the linear relationship

$$\cos(\theta/2) = \omega/\omega_p \quad , \qquad (2)$$

when b approaches zero. In Fig.1, θ vs $(\omega_p/\omega)^2$ are shown which are obtained from Eq.(1) for various b's. It is worthwhile noting that the differences between Eq.(1) and Eq.(2) are large near the cut-off density.

The electric field[6], E(z), does not necessarily fall off exponentially in the plasma, when the nonlinear skin effect occurs. Then, it is not practical to define the skin depth as the depth at which the field becomes 1/e of its surface value. Instead the skin depth d is defined[7] here by the slope of E(z) at the boundary z = 0 as

$$d = -E(0)\Big/\left.\frac{dE}{dz}\right|_{z=0} = \frac{1}{k_0}\cot\frac{\theta}{2} \quad , \qquad (3)$$

where k_o is the wavenumber in vacuum. Hence, the skin depth d can be known from the measurement of θ. It is obvious from Fig.1 and Eq.(3) that the skin depth d would increase with b for a given $(\omega_p/\omega)^2$.

When E(z) is relatively smaller than E_c, E(z) is expressed[6] as

$$E(z) = E_c\sqrt{2\left[1-(\omega/\omega_p)^2\right]}\,\operatorname{sech}\left[k_0 z\sqrt{(\omega_p/\omega)^2-1} - \Delta\right] \qquad (4)$$

where

$$\Delta = \ell n \frac{\sqrt{a}}{1+\sqrt{1-a}}\ , \quad a = b/\left[(\omega_p/\omega)^2 - 1\right]\left[1+\sqrt{1-2b/(\omega_p/\omega)^2}\right]$$

It is easily shown that $0 \leq a < 1$ and $\Delta < 0$. Equation (4) is the stationary envelope soliton whose half width and position x_p of the vertex are, respectively, given by the skin depth d in the cold plasma, i.e., $d = k_o^{-1}\left[(\omega_p/\omega)^2 - 1\right]^{-1/2}$, and $x_p = d\Delta < 0$. When b approaches zero, Eq.(4) tends to the exponential function given by the linear theory. The examples of the calculated E(z) from Eq.(4) are shown in Fig.2. It is obvious that the field in the plasma does not fall off exponentially, although Eq.(4) is not exact where $E(x) \approx E_c$.

In what follows, we modify the Silin's formula, Eq.(1), to include the longitudinal magnetic field, in order to compare with our experimental results obtained from the plasma in a waveguide. A microwave in a rectangular waveguide without plasma is a linearly polarized wave, which decomposes into right and left-hand circularly polarized waves, E_r and E_ℓ respectively, with identical phases in time. When the skin effects occur in the plasma for both waves, as in our experiment, the waveguide can be regarded as over-sized.[8] Then circularly polarized fields having different phases in time will exist in the plasma. Therefore, one can consider the phase shifts, θ_r and θ_ℓ, of the reflected waves from the plasma having right and left-hand circular polarizations, respectively, even though the

waveguide cross section is rectangular. Using the expressions for circularly polarized waves, $E_{r,\ell} = E_x \mp iE_y$, it is easily shown that the phase shift θ of a reflected wave, which is linearly polarized with the same direction of polarization as the incident wave, is given by

$$\cos^2\frac{\theta}{2} = \frac{1}{2}\left(\cos^2\frac{\theta_r}{2} + \cos^2\frac{\theta_\ell}{2}\right) . \qquad (5)$$

The angle θ in Eq.(5) is observed by a standing wave detector in the waveguide. In the linear theory, both waves can exist independently in the plasma, and their phase angles are given, by $\cos^2(\theta_{r,\ell}/2) = (1 \mp \omega_c/\omega)/(\omega_p/\omega)^2$, where ω_c is the electron cyclotron frequency. Substituting these expressions into Eq.(5), one directly obtains Eq.(2), which is independent of the applied magnetic field.[9]

When the nonlinear effect is included, the circularly polarized waves in the plasma are no longer independent of each other. Using an expression given by Gurevich and Pitaevskii,[10] we write, in our notation, the density correction factor, f(E), due to the radiation pressure as

$$f(E_r, E_\ell) = \exp\left[-\frac{1}{2E_c^2}\left(\frac{|E_r|^2}{1-\omega_c/\omega} + \frac{|E_\ell|^2}{1+\omega_c/\omega}\right)\right] , \qquad (6)$$

instead of Eq.(2.3) of Ref.6. Equation (6) results in a set of nonlinear differential equations[11] in E_r and E_ℓ which cannot be separated out unless some assumption is made about the field amplitudes. We therefore make three different

assumptions, i) $|E_\ell| >> |E_r|$, ii) $|E_r| = |E_\ell|$ and iii) $|E_r| >> |E_\ell|$ in the plasma. Consequently, we obtain[12] the following expression for θ in each case, using Eqs.(1), (5), (6) and $E_{r,\ell}(0) = 2E_i \cos(\theta_{r,\ell}/2)$, as

$$\text{i)}\quad \cos^2\frac{\theta}{2} \simeq -\frac{1}{2b}\left\{(1-\omega_c/\omega)\ln\left[1-\frac{b}{(\omega_p/\omega)^2-b}\right]+(1+\omega_c/\omega)\ln\left[1-\frac{b}{(\omega_p/\omega)^2}\right]\right\}, \quad (7)$$

$$\text{ii)}\quad \cos^2\frac{\theta}{2} = -\frac{1-(\omega_p/\omega)^2}{2b}\ln\left[1-\frac{b}{(1+\omega_c/\omega)(\omega_p/\omega)^2}\right]\left[1-\frac{b}{(1-\omega_c/\omega)(\omega_p/\omega)^2}\right], \quad (8)$$

and

$$\text{iii)}\quad \cos^2\frac{\theta}{2} \simeq -\frac{1}{2b}\left\{(1-\omega_c/\omega)\ln\left[1-\frac{b}{(\omega_p/\omega)^2}\right]+(1+\omega_c/\omega)\ln\left[1-\frac{b}{(\omega_p/\omega)^2-b}\right]\right\}. \quad (9)$$

Above three equations reduce to Eq.(2), as b approaches zero. Nonlinear effect due to non-zero b is emphasized in Eqs.(8) and (9).

It is well known that the characteristics of the waves in cold magnetoplasmas are summarized in the CMA diagram.[13] However, it has been based on the linear treatment of wave analysis. Hence, the diagram can be applied only for waves of small amplitudes. What will happen on the CMA diagram when the wave amplitude increases? Although this question is left, in general, unsolved at this moment, an example of the possible modifications on the diagram is here presented. Considerations are limited to the case of parallel propagation, i.e., k//B. Equation (1) can be modified for the circularly polarized waves incident on the plasma with uniform magnetic field which is applied perpendicular to the boundary. The phase angles of reflection coefficient are given[1-] by

$$\cos^2 \frac{\theta_{r,l}}{2} = -\frac{1 \mp \omega_c/\omega}{b} \ln\left[1 - \frac{b}{(\omega_p/\omega)^2}\right] . \qquad (10)$$

It is shown from Eq.(10) that the cut-off density is given by

$$(\omega_p/\omega)^2 = \frac{b}{1 - \exp[-b/(1 \mp \omega_c/\omega)]} , \qquad (11)$$

which becomes $(\omega_p/\omega)^2 = b$ for $b >> 1$. Then, the cut-off density is independent of the value of the magnetic field for strong incident powers. The cut-off lines calculated from Eq.(11) for various b's are shown in Fig.3. The upper and lower half planes correspond, respectively, to the right and left-hand circularly polarized waves. As is shown in Fig.3, the plane is divided into three regions A, B and C. The regions A, B and C correspond, respectively, to the whistler waves, the cut-off region and the fast electromagnetic waves. The border line between B and C is the cut-off line which is shown, in Fig.3, by the dashed line in the linear theory.[13] Equation (11) predicts that the cut-off line moves toward the high densities, when b increases.

A dominant nonlinear phenomenon associated with large amplitude whistler waves may be the amplitude oscillations[14] due to the particle trapping. The wavelength Λ of the amplitude oscillations is given[14] by

$$\Lambda = \frac{c}{\sqrt{n^3 \omega \xi \Omega_1}} \quad , \qquad (12)$$

where

$$n = \frac{cK}{\omega} \quad , \quad \xi = \frac{v_{te}}{c} \quad , \quad \Omega_1 = \frac{eB_1}{m} = \frac{e}{m}\sqrt{\frac{P\mu_0 n}{c}}$$

B_1 and P are, respectively, the magnetic field and the Poynting vector of the whistler waves. The experimental conditions, where the amplitude oscillations can be observed, are estimated in Fig.4. The oblique solid lines are the constant Λ lines in cm. The horizontal dashed lines are those where the attenuation distances $\Lambda_{col.}$ due to the collisions between electrons and ions are constant. The region where $\Lambda < 10$ (cm) and $\Lambda_{col.} > 10$ (cm) is shaded. The amplitude oscillations may be observed in the shaded region. In our experiment, $(\omega_p/\omega)^2 \simeq 1$ and P is several kW/cm. Then Λ is expected to be larger than 10 cm. The amplitude oscillations cannot be observed in our experiment.

III. EXPERIMENTAL RESULTS

A steady-state highly-ionized plasma[15] of the Institute of Plasma Physics, Japan is used in our experiment. The plasma is produced between a hot cathode and a water cooled anode in helium at a pressure of a few Torr. The plasma is introduced into a glass chamber through a small hole in the anode. The chamber is differentially evacuated to the pressure of 10^{-3} Torr. A uniform magnetic field B of

several thousand Gauss is applied axially to keep the electron density high. The values of the plasma density N_e (cm^{-3}) and the electron temperature T_e(eV) vs the discharge current I_d (A) are shown in Fig.5. The electron densities measured by the Langmuir probe just in front of the target are in agreement, within a factor, with those obtained from the microwave reflections[3] for a small incident power. A standard X-band rectangular waveguide with a water cooled target is inserted axially into the plasma. A schematic diagram, how the skin depths in the waveguide are measured, is shown in Fig.6. A quartz block of 1.1 cm thickness is placed in the waveguide to make the plasma boundary clear and sharp. The plasma in the waveguide seems to be uniform in the axial direction, because the experimental results are insensitive to the position of the quartz. Microwave pulses of 15 kW and time width τ = 1.2 μsec at a frequency of 9.37 GHz are launched into the plasma repeatedly through the power divider and the standing wave detector.

The reflected powers from and the transmitted powers through the plasma are measured for an incident power at different values of B. The transmitted power is detected by a small wire antenna which is moved in the axial direction in front of the target. An example is shown in Fig.7. Both signals are small near the electron cyclotron resonance at $B = B_c = 3345$ (G). Thus, the microwaves are absorbed in the plasma at the resonance. The propagation of whistler waves with little attenuation is observed, when $B > B_c$.

The wave patterns are recorded using the usual microwave-interferometer circuit and the boxcar integrator. The example of the patterns with and without plasmas is shown in Fig.8. The dispersion relation of the observed waves is plotted in Fig.9. The solid lines are the calculated dispersion relations of whistler waves in a cold plasma. The dashed lines are calculated ones where the effects of the left-hand circularly polarized field E_ℓ are taken into account. Since the observed values are close to the solid lines rather than the dashed lines, the effect of E_ℓ can be neglected. In our experiment, the wave is excited by the waveguide into the plasma. The waves seem to be excited very effectively, since the reflected powers from the plasma are considerably small for $\omega_c/\omega > 1$, as is shown in Fig.7. It is confirmed that the wavelengths and the attenuations of the whistler waves are unchanged for a wide range of incident powers. The collisional damping of the waves can be completely neglected. The attenuation observed near the cyclotron resonance is due to the cyclotron damping.

The experiment on the skin effects is carried out in a magnetic field $2800 < B < 3050$, where the low-level incident microwaves are almost totally reflected from the plasma for N_e greater than the cut-off density. The standing wave patterns observed by a crystal detector through a slotted section are recorded using a boxcar integrator. Next, the plasma is replaced by a movable metal short plunger, whose position simulates the density of the plasma. Since the quartz is used before the plunger and/or the

plasma, the standing waves do not move linearly when the position of the plunger is changed. Calibrating for the nonlinearity of the shifts, the phase angles of reflection from the plamsa are derived. The result is shown in Fig.10. The phase angle decreases for a given B and I_d, as the incident power increases. When the neutral pressure is increased to 10^{-1} Torr, the change of θ is in opposite way to that in Fig.10, with increase in incident power, because of the additional ionization by the powerful microwaves. This is the reason why we conclude that the results in Fig.10 are clearly due to the nonlinear skin effect.

In Fig.11, the experimental results of the skin effect are compared with the theoretical predictions for b = 0.167 (thick dashed lines) and 0.230 (thick chained lines), which correspond, respectively, to 2.9 kW and 4.0 kW of incident powers at T_e = 8 (eV). The solid line is the linear relationship calculated from Eq.(2). Calculated lines from Eqs.(7) and (9) are not shown, since they are very close to the solid line. Equation (8) is the closest to the experimental values among the three equations. This suggests that the assumption $|E_r| = |E_\ell|$, from which Eq.(8) is derived, holds approximately in our experiment. In other words, the result suggests that an enhanced penetration of E_r occurs in the plasma for the high power incident microwaves, since the inequality $|E_r| < |E_\ell|$ holds at the cut-off region for both the waves in the linear theory.

Using the boxcar integrator, the plasma parameters N_e and T_e are measured by the Langmuir probe for various periods after the incidence of the high power microwave

pulse. The examples of the probe characteristics are shown in Fig.12. An example of the plasma parameters vs time obtained from the probe characteristics is shown in Fig.13, where the microwave pulse of 15 kW becomes transparent even for $(\omega_p/\omega)^2 > 1$. The probe measurement will be reliable even in the microwave field, since the high frequency drift velocity of electrons, $eE/m\omega$, in the plasma is much smaller than the electron thermal velocity. During the incidence of the microwave pulse, N_e decreases considerably from the steady state value.[16] This fact is further evidence of the nonlinear skin effect.

IV. DISCUSSIONS

In our experiment, the skin depths, which are of the order of a few mm, are much greater than v_{te}/ω and/or v_{ti}/ω, where v_{te} and v_{ti} are the thermal velocities of electrons and ions, respectively. On the other hand, the skin depths are much smaller than $v_{te}\tau$ and smaller than $v_{ti}\tau$, where τ is the time width of the microwave pulse. Therefore, Eq.(6) can be reasonably applied[10] to our experiment.

Gurovich and Karpman[17] analysed an electromagnetic envelope soliton propagating in a high density plasma. In a limiting case, they obtained an expression of the electric field in the plasma for the stationary soliton that is just the same as the nonlinear skin effect[6], i.e., Eq.(4). Our experimental results, that the skin depths are dependent on the incident power, suggetst the existence of an electro-

magnetic field in the plasma similar to the stationary envelope soliton.

We believe that the modification of the CMA diagram presented in Fig.3 can be observed experimentally, since it is a generalized version of the nonlinear skin effect verified in the present article.

REFERENCES

1. H. Dreicer, D. B. Henderson and J. C. Ingraham, Phys. Rev. Rett. 26, 1616 (1971)
2. M. Porkolab, V. Arunasalam and R. A. Ellis, Jr., Phys. Rev. Lett. 29, 1438 (1972)
3. I. R. Gekker and O. V. Sizukhin, Pis'ma Zh. Eksp. Teor. Fiz. 9, 408 (1969) [JETP Lett. 9, 243 (1969)]
4. P. Kaw, E. Valeo and J. M. Dawson, Phys. Rev. Lett. 25, 430 (1970)
5. S. Takeda and M. Roux, J. Phys. Soc. Japan 16, 95 (1961)
6. V. P. Silin, Zh. Eksp. Teor. Fiz. 53, 1662 (1967) [Sov. Phys. JETP 26, 955 (1968)]
7. E. S. Weibel, Phys. Fluids 10, 741 (1967)
8. When the densities are greater than the cut-off density, the skin depths in the plasma are considerably smaller than the side dimensions of the waveguide. In theoretical treatments, the skin effects in the waveguide are the same as those in free space. However, the waveguide wavelength should be adopted in the waveguide without plasma instead of that in free space. This fact, which results in a decrease of the cut-off density, is taken into account in our experiment. The theoretical treatments cannot be simplified even in a circular waveguide as long as a linearly polarized microwave is incident on the magnetized plasma.
9. This prediction is not completely verified in our experiments, since the electron density changes as the magnetic field changes.

10. A. V. Gurevich and L. P. Pitaevskii, Zh. Eksp. Teor. Fiz. 45, 1243 (1963) [Sov. Phys. JETP 18, 855 (1964)]

11. H. Motz and C. J. H. Watson, in Advances in Electronics and Electron Physics, Edited by L. Marton (Academic, New York, 1967) Vol.23, p.225, Eq.(7)

12. The value of b in Eq.(1) is modified, respectively, to $b/(1 \mp \omega_c/\omega)$, when the strong field causing the radiation pressure is E_r or E_ℓ. Similarly, $(\omega_p/\omega)^2$ in Eq.(1) is modified, respectively, to $(\omega_p/\omega)^2/(1 \mp \omega_c/\omega)$, when the skin effect is concerned with E_r or E_ℓ. See Ref.11.

13. W. P. Allis, S. J. Buchsbaum and A. Bers, "Waves in Anisotropic Plasmas" (M.I.T. Press, Cambridge, Massachusetts, 1963)

14. P. Parmadesso and G. Schmidt, Phys. Fluids 14, 1411 (1971)

15. The plasma is called "TPD-plasma" which is abbreviated for the Test Plasma of DC Discharge.

16. I. R. Gekker, E. Ja. Holz, B. P. Kononov, K. A. Sarksian, V. A. Silin and L. E. Tsopp, in Proceedings of the 7th International Conference on Phenomena in Ionized Gases, Beograd, 1965, Part II, p.445

17. V. Ts. Gurovich and V. I. Karpman, Zh. Eksp. Teor. Fiz. 56, 1952 (1969) [Sov. Phys. JETP 29, 1048 (1969)]

FIGURE CAPTIONS

Fig.1. Calculated values of the phase angle θ of reflection coefficient vs $(\omega_p/\omega)^2$ from Eq.(1).

Fig.2. Field patterns in the plasma calculated from Eq.(4) for various b's.

Fig.3. A modified CMA diagram for the parallel propagation (k // B).

Fig.4. Experimental conditions at which the amplitude oscillations can be observed. Appropriate region is shaded.

Fig.5. Measured values of N_e (cm^{-3}) and T_e (eV) vs I_d (A).

Fig.6. Block diagram of the experimental set up.

Fig.7. Measured $|R|^2$ and $|T|^2$ vs B (Gauss). $|R|^2$ and $|T|^2$ are not calibrated for each other.

Fig.8. Observed patterns with and without the plasma.

Fig.9. Dispersion relation of observed waves. The solid and dashed lines are the calculated values of whistler waves.

Fig.10. Measured values of θ vs discharge current I_d for various incident powers. Experimental set up where the skin depths in the waveguide are measured is shown in the inset.

Fig.11. Comparison of the experimental results with the theoretical predictions for the variation of θ vs $(\omega_p/\omega)^2$. O —— a small power of the order of 10 mW, adjusted to the theoretical line for b = 0, ▲ —— 2.9 kW to be compared with the thick dashed

lines (b = 0.167), ● —— 4.0 kW to be compared with the thick chained lines (b = 0.230).

Fig.12. Examples of Langmuir probe characteristics with and without microwave pulse, which is incident during $0 \leq t \leq 1.2$ μsec.

Fig.13. Change of the plasma parameters due to the incidence of high power microwaves.

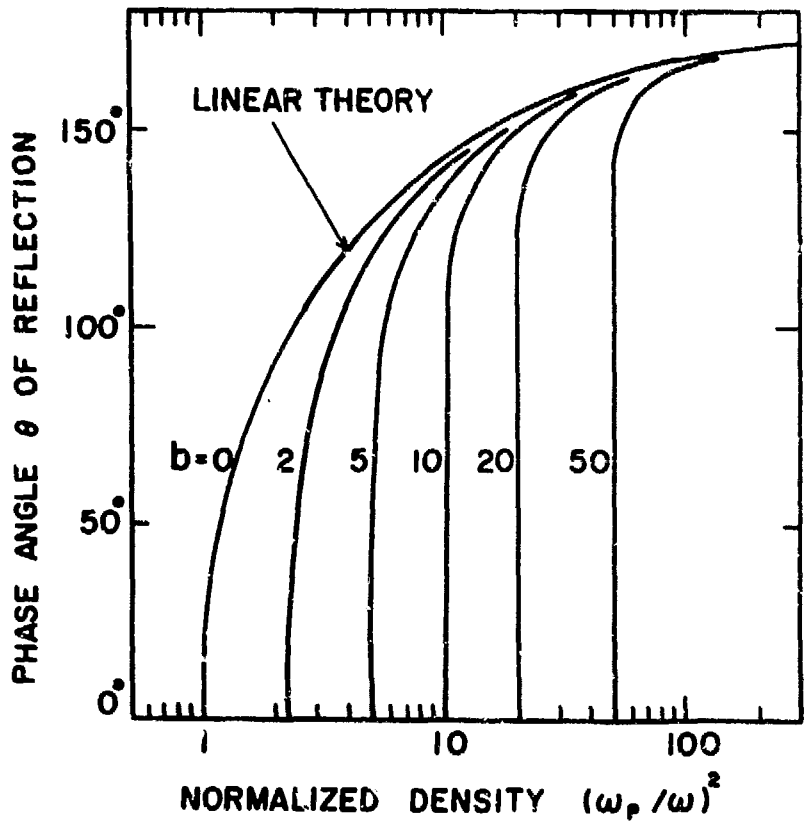
LINEAR THEORY
150°
100°
50°
0°
b=0
2
5
10
20
50
1
10
100
PHASE ANGLE θ OF REFLECTION
NORMALIZED DENSITY $(\omega_p/\omega)^2$

Fig.1

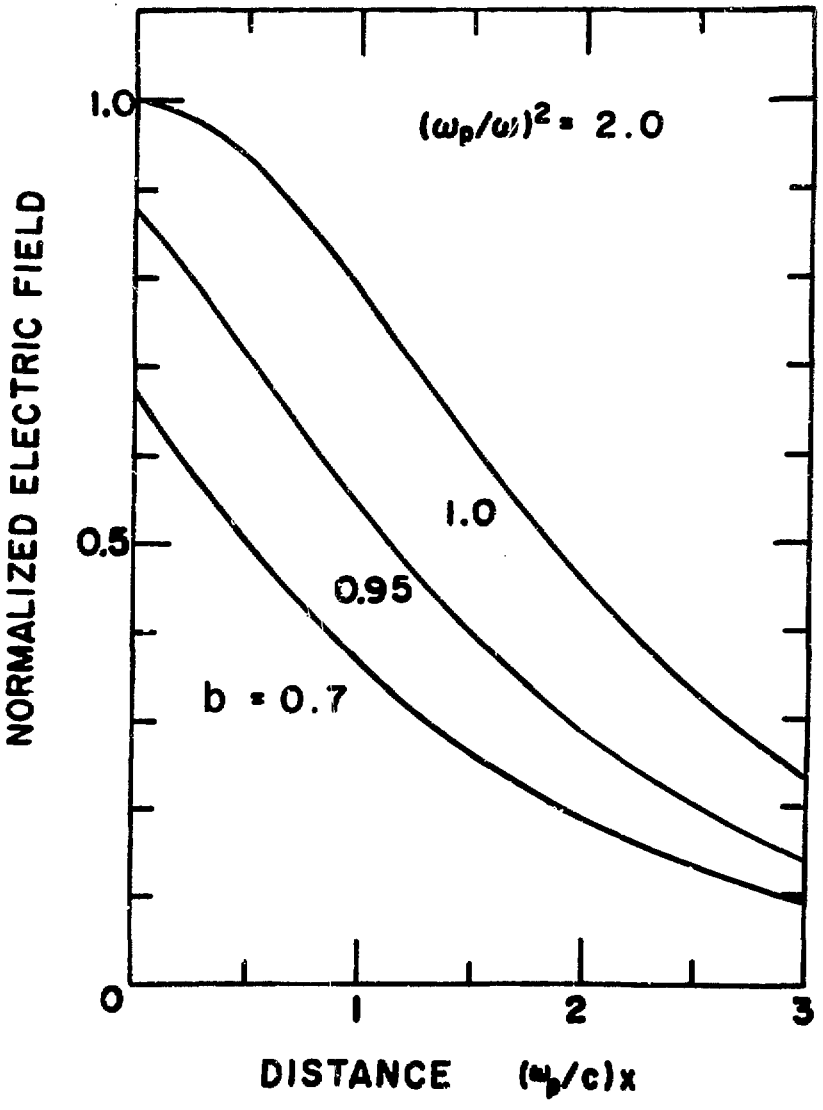
NORMALIZED ELECTRIC FIELD
1.0
0.5
0
$(\omega_p/\omega)^2 = 2.0$
1.0
0.95
b = 0.7
1
2
3
DISTANCE $(\omega_p/c)x$

Fig.2

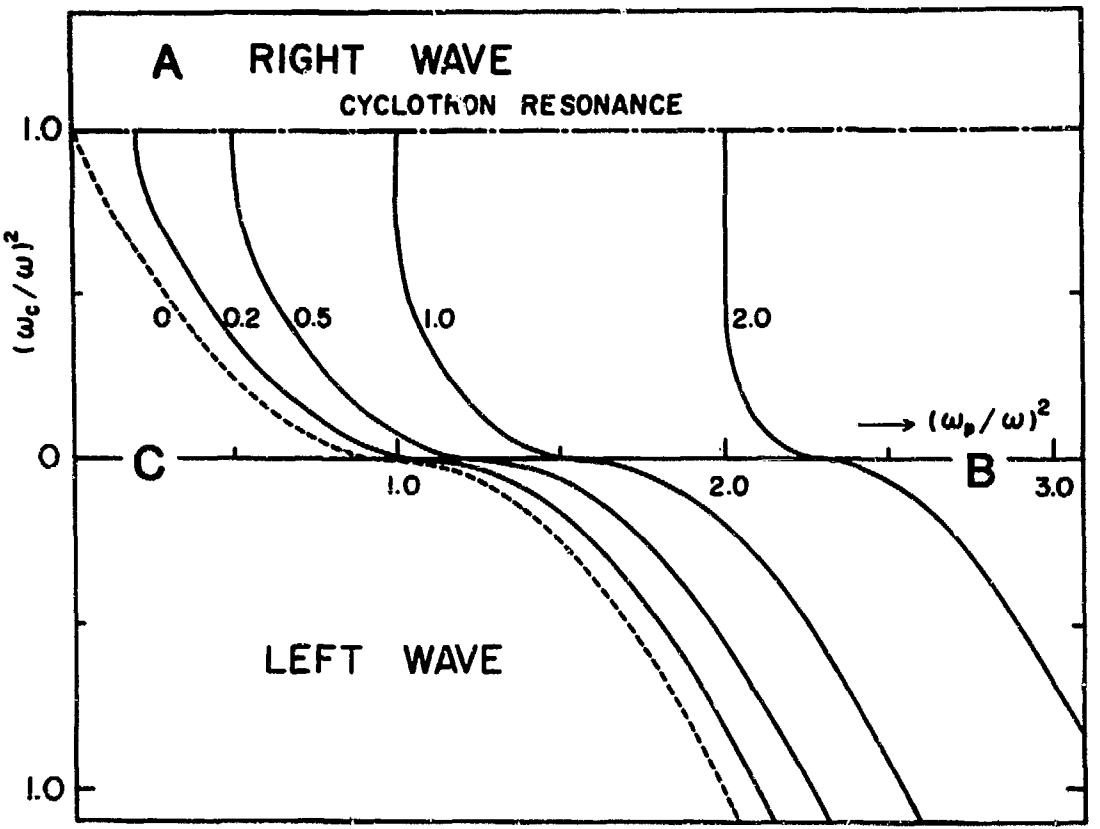
A
RIGHT WAVE
CYCLOTRON RESONANCE
1.0
0
1.0
$(\omega_c/\omega)^2$
0
0.2
0.5
1.0
2.0
$\rightarrow (\omega_p/\omega)^2$
C
B
1.0
2.0
3.0
LEFT WAVE

Fig.3

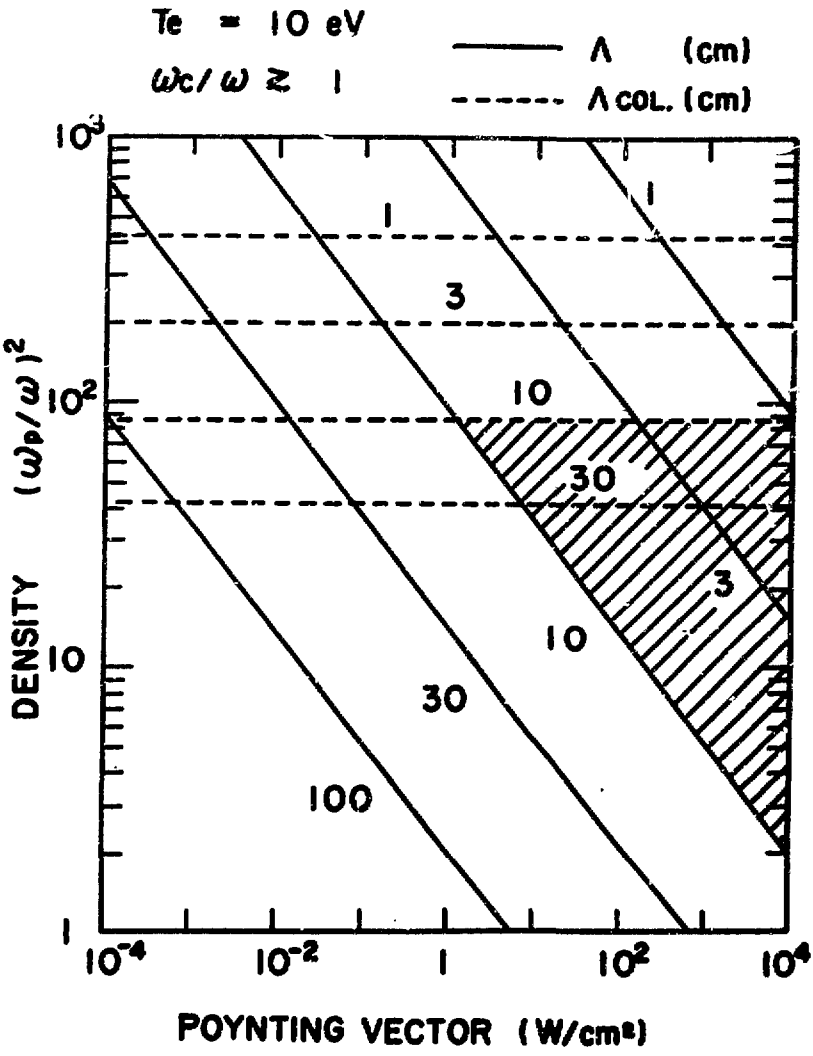
Te = 10 eV
ωc/ω ≥ 1
Λ (cm)
Λ COL. (cm)
DENSITY (ωp/ω)²
POYNTING VECTOR (W/cm²)
10³
10²
10
1
10⁻⁴
10⁻²
1
10²
10⁴
1
3
10
30
100
1
3
10
30

Fig.4

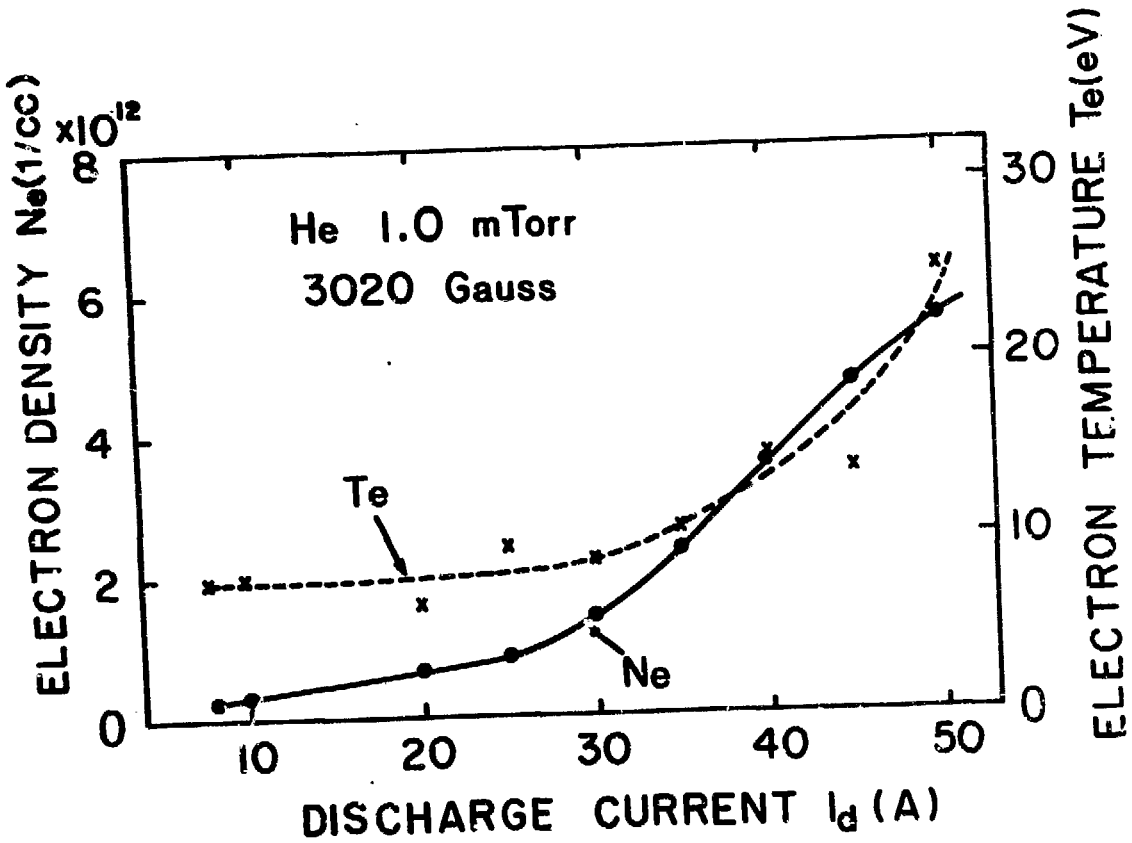
ELECTRON DENSITY Ne(1/cc)
x10^12
8
6
4
2
0
He 1.0 mTorr
3020 Gauss
Te
Ne
10
20
30
40
50
DISCHARGE CURRENT Id (A)
30
20
10
0
ELECTRON TEMPERATURE Te(eV)

Fig.5

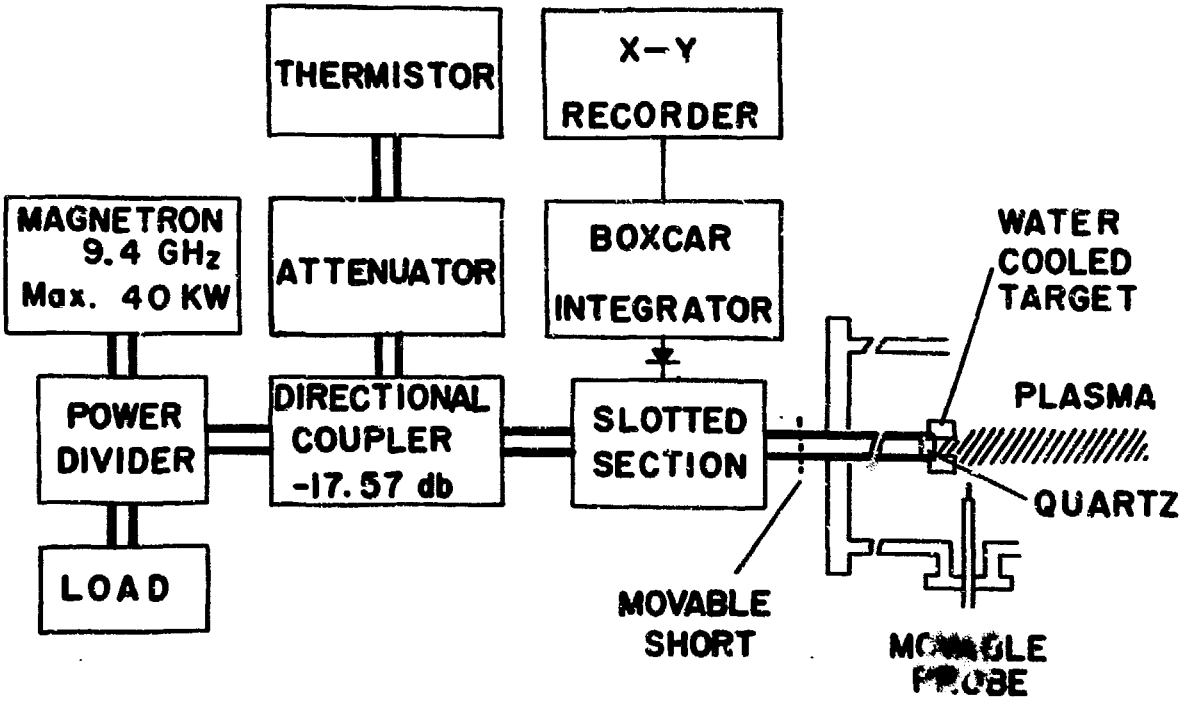
THERMISTOR
X–Y
RECORDER
MAGNETRON
9.4 GHz
Max. 40 KW
ATTENUATOR
BOXCAR
INTEGRATOR
WATER
COOLED
TARGET
PLASMA
POWER
DIVIDER
DIRECTIONAL
COUPLER
-17.57 db
SLOTTED
SECTION
QUARTZ
LOAD
MOVABLE
SHORT

Fig.6

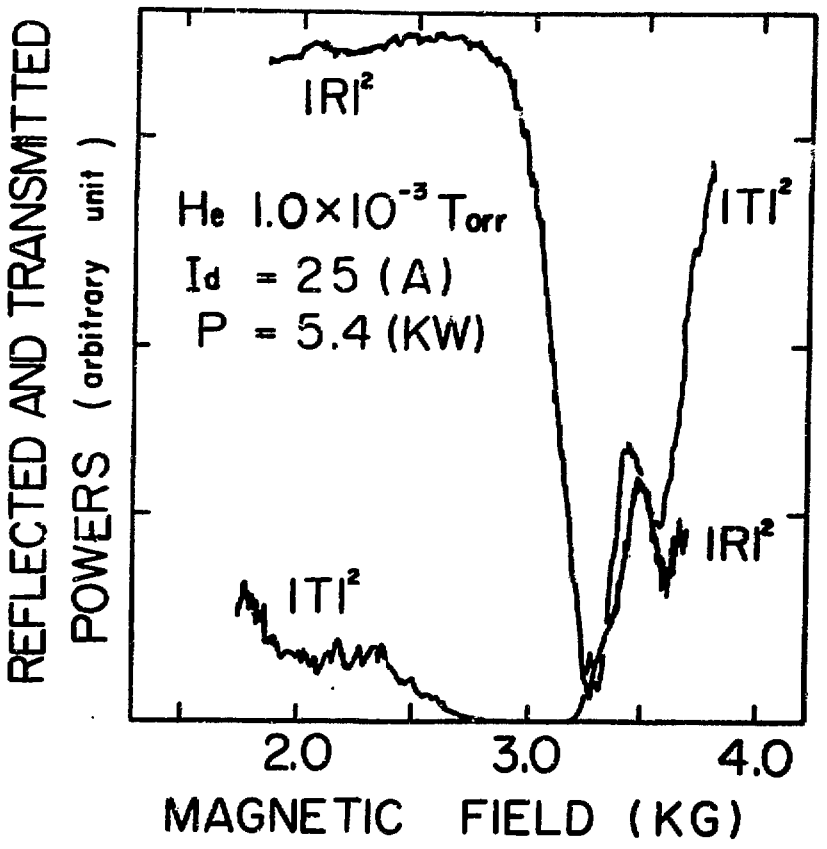
REFLECTED AND TRANSMITTED POWERS (arbitrary unit)
|R|²
He 1.0×10⁻³ Torr
Id = 25 (A)
P = 5.4 (KW)
|T|²
|T|²
|R|²
2.0
3.0
4.0
MAGNETIC FIELD (KG)

Fig.7

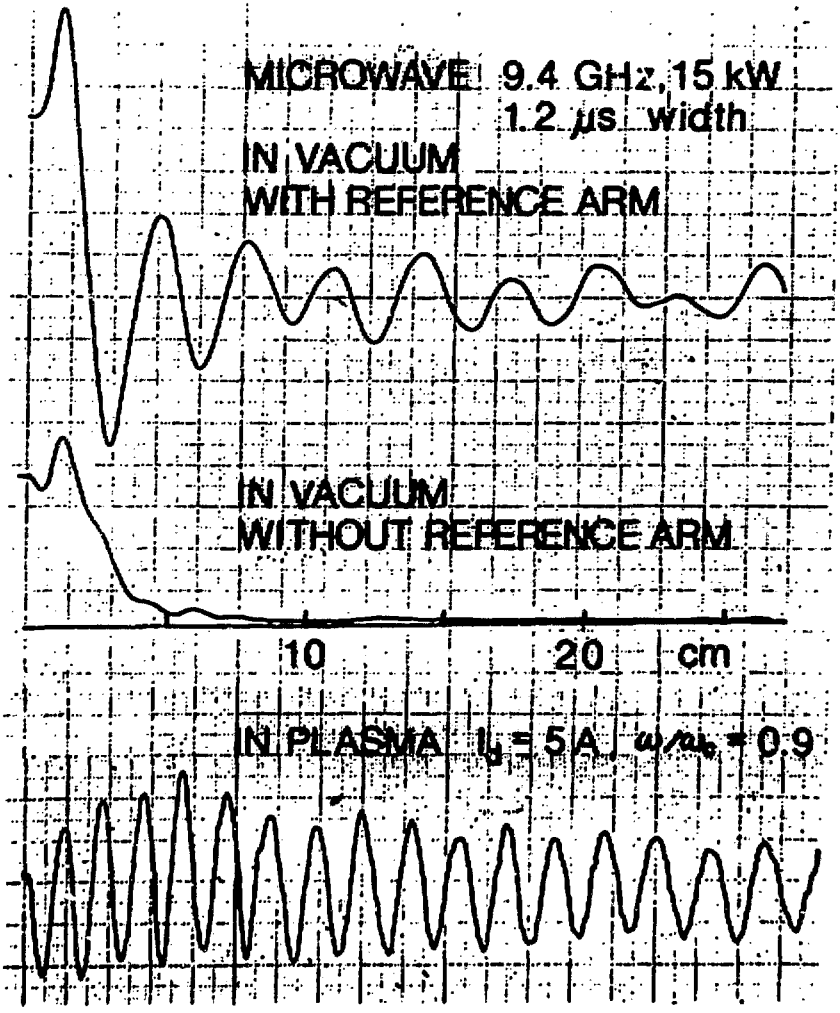
MICROWAVE 9.4 GHz, 15 kW
1.2 μs width
IN VACUUM
WITH REFERENCE ARM
IN VACUUM
WITHOUT REFERENCE ARM
10
20
cm
IN PLASMA I_d = 5 A ω/ω_c = 0.9

Fig.8

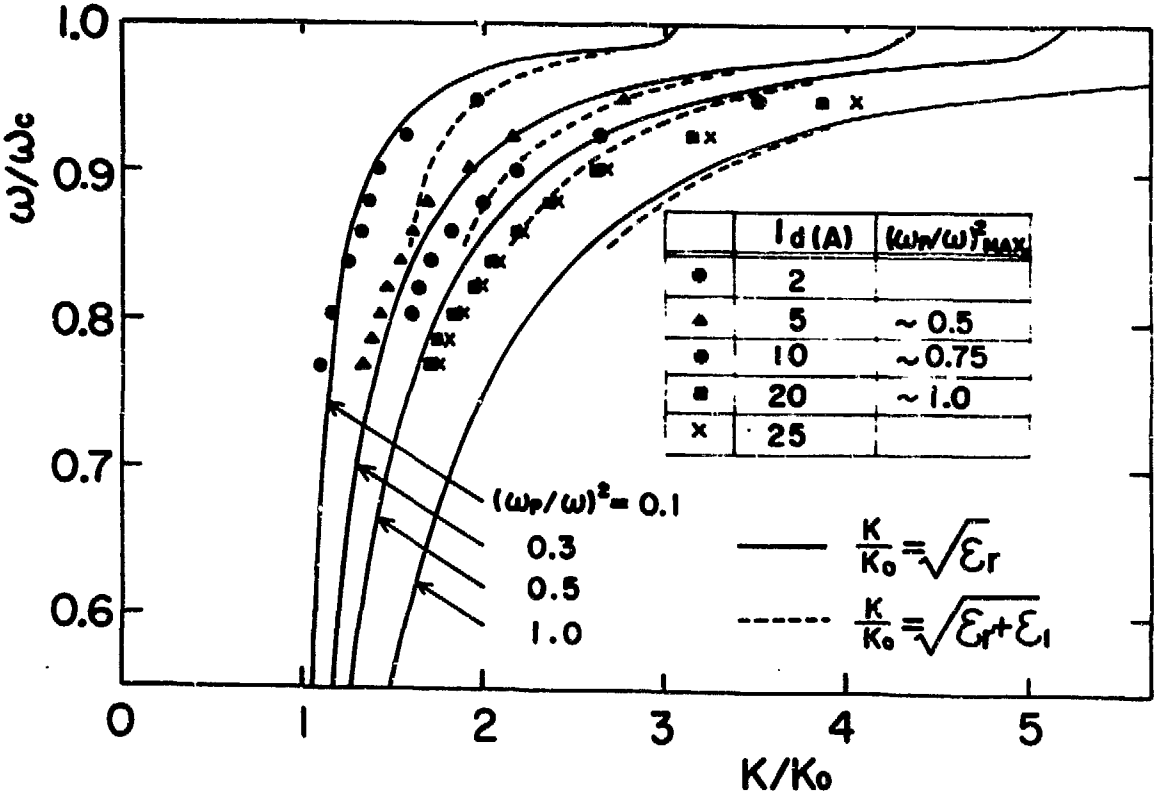
1.0
0.9
0.8
0.7
0.6
ω/ωc
0
1
2
3
4
5
K/K₀
	I_d (A)	$(\omega_p/\omega)^2_{MAX}$
●	2	
▲	5	~ 0.5
●	10	~ 0.75
■	20	~ 1.0
×	25	
$(\omega_p/\omega)^2$ = 0.1
0.3
0.5
1.0
$\frac{K}{K_0} = \sqrt{\varepsilon_r}$
$\frac{K}{K_0} = \sqrt{\varepsilon_r + \varepsilon_i}$

Fig.1

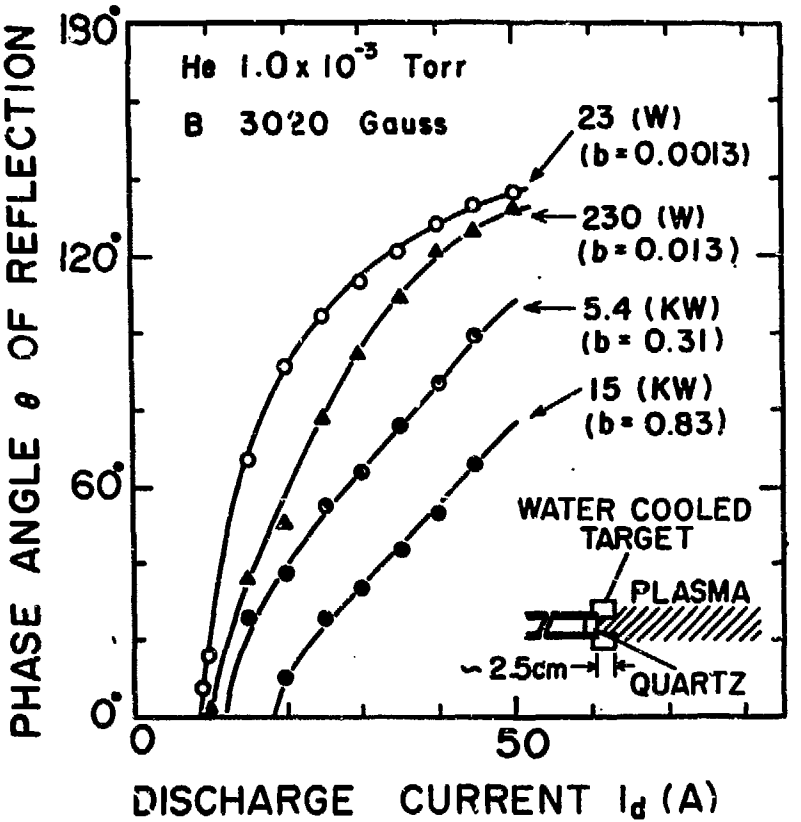
He 1.0 x 10⁻³ Torr
B 3020 Gauss
23 (W)
(b = 0.0013)
230 (W)
(b = 0.013)
5.4 (KW)
(b = 0.31)
15 (KW)
(b = 0.83)
WATER COOLED
TARGET
PLASMA
~2.5cm
QUARTZ
PHASE ANGLE θ OF REFLECTION
180°
120°
60°
0°
0
50
DISCHARGE CURRENT I_d (A)

Fig.10

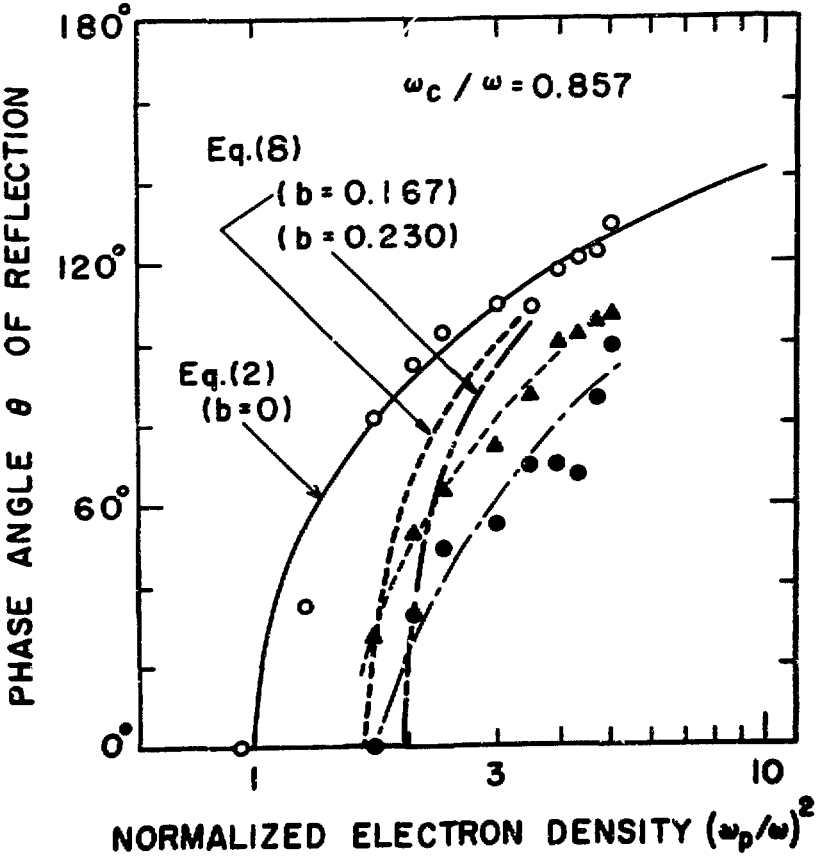
180°
120°
60°
0°
PHASE ANGLE θ OF REFLECTION
ωc / ω = 0.857
Eq.(8)
(b = 0.167)
(b = 0.230)
Eq.(2)
(b = 0)
1
3
10
NORMALIZED ELECTRON DENSITY (ωp/ω)²

Fig.11

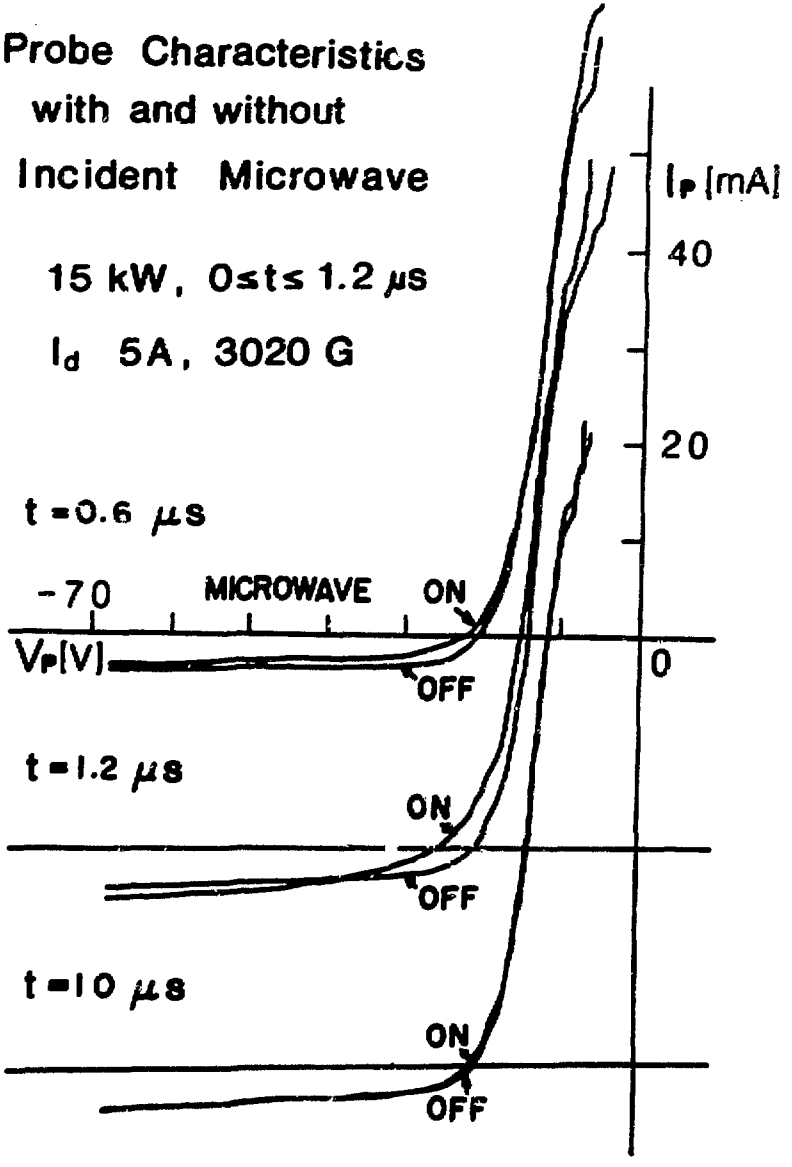
Probe Characteristics
with and without
Incident Microwave
15 kW, 0≤t≤ 1.2 μs
I_d 5A, 3020 G
I_P [mA]
40
20
t =0.6 μs
-70
MICROWAVE
ON
V_P[V]
OFF
0
t =1.2 μs
ON
OFF
t =10 μs
ON
OFF

Fig.12

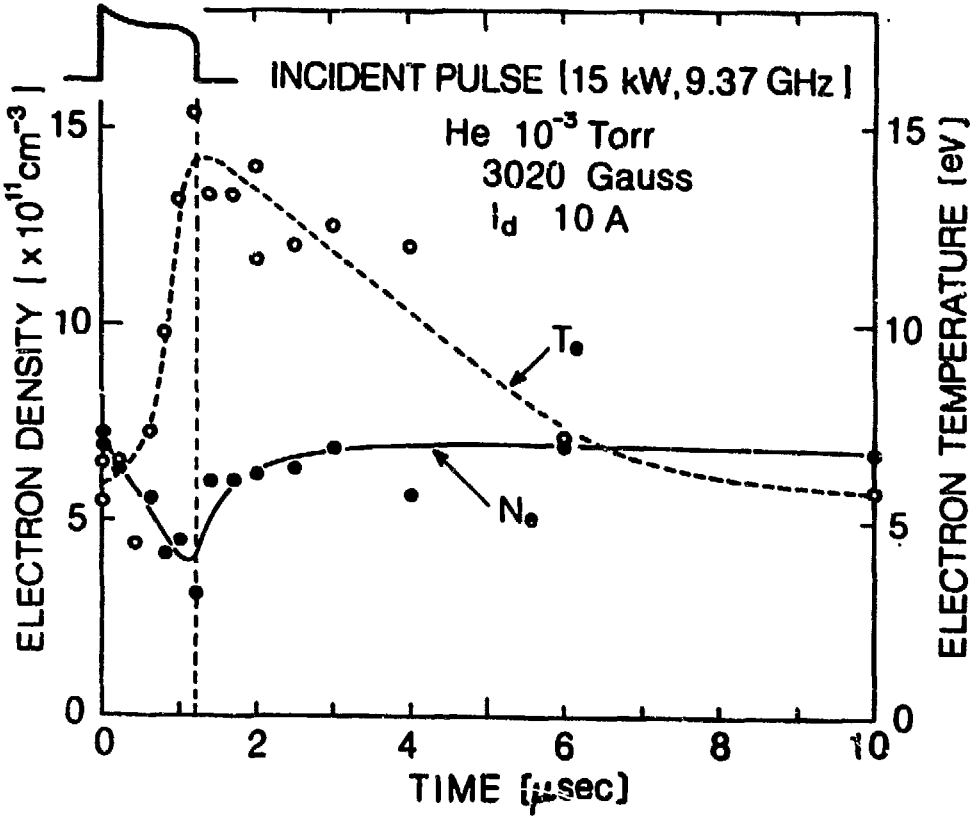
INCIDENT PULSE [15 kW, 9.37 GHz]
He 10^{-3} Torr
3020 Gauss
I_d 10 A
T_e
N_e
ELECTRON DENSITY [$\times 10^{11} cm^{-3}$]
ELECTRON TEMPERATURE [eV]
TIME [μsec]
0
5
10
15
0
2
4
6
8
10

Fig.13

ERRATA

Page	Line	Incorrect	Correct
Text			
5	1	where E (x)	when E (z)
9	14	kW/cm	kW/cm^2
12	14	lines	line
12	14	lines	line
13	last	suggetst	suggest
Reference			
15	2	Rett.	Lett.
Figure Captions			
18	1	lines	line
18	2	lines	line
Figure No.2		$(\omega_p/c)x$	$(\omega_p/c)z$